

Metal-Mediated Inhibition of *Escherichia coli* Methionine Aminopeptidase: Structure–Activity Relationships and Development of a Novel Scoring Function for Metal–Ligand Interactions

Rolf Schiffmann, Alexander Neugebauer, and Christian D. Klein*

Saarland University, FR 8.5 Pharmaceutical and Medicinal Chemistry, D-66041 Saarbrücken, Germany

Received May 20, 2005

We report the discovery of thiabendazole as a potent inhibitor ($K_i = 0.4 \mu\text{M}$) of *Escherichia coli* methionine aminopeptidase (ecMetAP) and the synthesis and pharmacological evaluation of thiabendazole congeners with activity in the upper nanomolar range. Elucidation of the X-ray structure of ecMetAP in complex with thiabendazole and an unrelated inhibitor that was independently described by another group showed that both compounds bind to an additional Co^{II} ion at the entrance of the active site. This unexpected finding explains the inactivity of the compounds under *in vivo* conditions. It also allows us to discuss the structure–activity relationships of this series of compounds in a meaningful way, based upon docking runs with an auxiliary metal ion. We describe a new scoring function for the evaluation of metal-mediated inhibitor binding that, unlike the previously used scoring function implemented in the docking program, allows us to distinguish between active and inactive compounds. Finally, conclusions for the structure-based design of *in vivo*-active inhibitors of ecMetAP are drawn.

Introduction

Infectious and parasitic diseases are responsible for 20% of the mortality worldwide, followed by malignant neoplasms with about 13%.¹ The emergence of antibiotic-resistant bacteria is nowadays a serious challenge to the clinical treatment of infections. Drug resistance is also a problem in the treatment of cancer. Methionine aminopeptidases (MetAPs) are target proteins for the development of both anticancer and antibacterial compounds. MetAPs are ubiquitous metal-dependent enzymes involved in the N-terminal processing of proteins and have been characterized for *Escherichia coli*,² *Salmonella typhimurium*,³ baker's yeast,³ humans,^{4,5} and other species. Protein synthesis is normally initiated with the AUG triplet coding for methionine (in the cytosol of eukaryotes) or N-formyl-methionine (in prokaryotes, mitochondria, and chloroplasts). For a significant fraction of the intracellular proteins, the amino-terminal methionine is removed by MetAPs after the initiation of translation. This process is mostly dependent on the adjacent residue² and essential for further processing such as acetylation or myristoylation. Thus MetAPs play a key role in the functional regulation of proteins. The physiological importance of MetAP activity is underscored by the nonviability of organisms where all MetAP genes have been deleted or all MetAP gene products are inhibited. This has been shown for *E. coli*, *S. typhimurium*, and *Saccharomyces cerevisiae*.^{6–8}

Two isoforms of MetAPs can be distinguished: type 1 and type 2. The latter contains an insert in the C-terminal domain whose function is still unknown. Eubacteria have only type 1 MetAP, archaeobacteria possess only type 2, and eukaryotes express both types.⁹ Eukaryotic MetAPs have N-terminal extensions involved in ribosome association. However, the active site is conserved among all MetAPs known so far. Two divalent transition-metal ions are ligated by five active site residues (two aspartates, two glutamines, and a histidine) as can be seen in the crystal structure. One water molecule (or hydroxide ion)

bridges the two metal ions. In recent studies, the protonation states of MetAPs have been examined in our group by theoretical and experimental methods.¹⁰ In short, the binding of irreversible inhibitors of the epoxide type depends on the presence of a metal-bound, acidic water molecule in the active site. This proton-donating water molecule is predominantly present at acidic pH. In contrast, the hydrolysis of the substrate (nucleophilic attack on the amide bond carbonyl carbon) is initiated by a hydroxide ion. Since the pH optimum for catalytic activity is around pH 7.5, one can assume that the active site of MetAPs contains a metal-bound hydroxide ion at physiological pH. The virtual screening experiments, which constitute a part of the work presented here, were therefore performed on an active site with a hydroxide ion located between the two metal ions.

MetAPs are considered to be dinuclear Co^{II} -dependent enzymes because Co^{II} reliably activates all known MetAPs. Activity has also been observed with other metal ions, depending on the type and origin of MetAP, assay conditions, and substrate used. Apart from Co^{II} , also Zn^{II} ,¹¹ Mn^{II} ,¹² Fe^{II} ,¹³ and Ni^{II} ¹⁴ have been proposed to be the relevant metal ion. Thus, the identity of the *in vivo* metal ions is still contentious, but Co^{II} is generally used for *in vitro* screening of inhibitors. The active site of the *E. coli* MetAP crystallized in the presence of Mn^{II} aligns very well with that of the di- Co^{II} form, indicating no major changes in geometry upon the replacement of Co^{II} by Mn^{II} .¹⁵ However, although the identity of the metal ion does not seem to have an impact on the geometry of the active site, it is clearly important for the development of inhibitors.

Irreversible, MetAP-2-selective inhibitors such as fumagillin and its derivative TNP-470 contain an epoxide moiety that covalently binds to a histidine residue at the entrance of the active site. Fumagillin, a natural product isolated from *Aspergillus fumigatus*, was originally identified as an antibacteriophagic¹⁶ and amebicidal agent^{17,18} but was by chance rediscovered in 1990¹⁹ as an inhibitor of angiogenesis.¹⁹ TNP-470 has been evaluated in clinical studies as an anticancer agent.

The competitive inhibitors are generally metal-complexing substances with a variety of functional groups. A class contain-

* Corresponding author. E-mail: cdpk@mx.uni-saarland.de. Mailing address: Pharmaceutical and Medicinal Chemistry, Saarland University FR 8.2, P.O. Box 151150, D-66041 Saarbrücken, Germany. Phone: ++49-681-302-2924. Fax: ++49-681-302-4386.

ing a triazole group as the metal ligand has been described.^{12,20,21} Other (peptidic) compounds utilize a hydroxamic acid group to chelate the metal ions.²² Small molecule inhibitors based on pyridine-2-carboxylic acid thiazol-2-ylamide (see structure **42**, Table 5)²³ and on thiazole-2-oxalamide are known, apart from 5-phenylfuran-2-carboxylic acid derivatives.¹⁵ Recently, Douan-gamath and co-workers have identified two series of inhibitors, α -keto heterocycles and aminoketones, that bind as transition-state analogues (see structures **44–46**, Table 5).²⁴

Other competitive inhibitors mimic peptide substrates and contain, for example, an α -hydroxy- β -aminoacyl (bestatin) group.²⁵ The bengamides (a marine natural product isolated from sponges) and synthetic analogues thereof²⁶ also belong to this class.

Although type 1 MetAPs seem to play a bigger role in methionine metabolism, the two types of MetAPs can generally substitute for each other. The fact that bacteria express only type 1 MetAPs makes this enzyme a target for the development of new antibiotic drugs. Besides, insight into the mode of action of inhibitors and characterization of the enzyme not only will be useful for the further development of drugs but also will lead to a better understanding of the physiological processes involved in the development of cancer and in cancer growth.

Our own work in this field has been focused on the selectivity mechanisms of MetAP inhibitors and a detailed study of those properties of the active site that govern its small-molecule binding behavior. One of the results of the latter work was an active site model for the ecMetAP with ab initio partial atomic charges and partially deprotonated water molecules, which were used as receptor structures for virtual screening purposes.^{10, 27}

In this paper, we report the discovery of thiabendazole as a potent inhibitor of ecMetAP by virtual screening methods and the subsequent synthesis and testing of thiabendazole analogues to gain insight into structure–activity relationships. These results, together with the binding mode of thiabendazole determined by X-ray crystallography as previously reported,²⁸ were used to develop a novel scoring function called Turboscore. This scoring function is specifically tailored for metal–ligand interactions and shown to be effective in distinguishing active from inactive compounds.

Results and Discussion

Virtual Screening. Virtual high-throughput screening was performed using the program GOLD. Two receptor structures, both based on the published X-ray structure 2MAT, were used in the virtual screening runs. One of the structures contained, in addition to the protein and the metal ions, a bridging hydroxide ion and a fully protonated, singly coordinated water molecule. Since we expected that ligands can also replace the water/hydroxide molecules and bind directly to the metal ions, a second screening run was performed on a completely unsolvated active site. The receptor structure is shown schematically in Figure 1.

The standard GOLD zinc parameters were used for the metal ions. Partial atomic charges for the active site atoms were as described in ref 10. The virtual screening was performed on the public “NCI Open” database and on our proprietary in-house database of drugs and other small molecules. Using the GOLD “database screening” settings, we saved the 1000 best-ranked compounds and subsequently analyzed them by visual inspection. In the virtual screening run without chelated water molecules, a clear preference for ligands with annealed, planar heterocyclic systems could be observed. These compounds fit neatly into the MetAP active site without waters. In contrast,

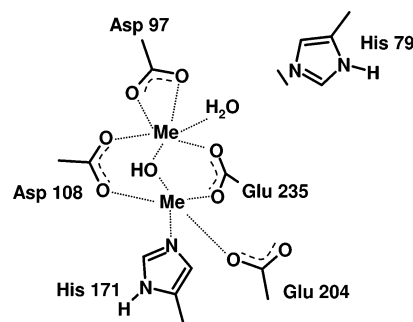


Figure 1. Active site of *E. coli* MetAP. Two receptor structures were used for the virtual screening runs, one with the hydroxide/water ligands as shown and one without them. Me = metal ion (cobalt in the X-ray structure, zinc in the virtual screening runs).

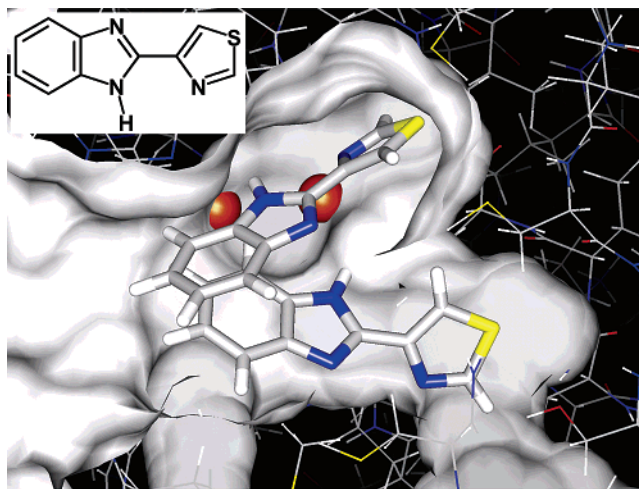


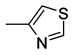
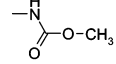
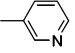
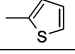
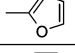
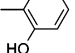
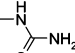
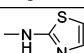
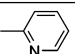
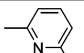
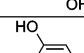
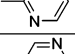
Figure 2. The two docking poses of thiabendazole in the nonsolvated *E. coli* MetAP active site. The two metal ions are shown as red spheres. This picture was generated using the Chimera software.²⁹

the “hydrated” active site is too narrow for such ligands. Among the top-scoring compounds in the nonsolvated active site, we identified the known anthelmintic and antimycotic drug thiabendazole. The structural formula and the two poses (generated by the docking software) of thiabendazole in the MetAP active site are shown in Figure 2.

One can clearly see that there is a good steric fit between thiabendazole and the MetAP active site and that the thiabendazole heteroatoms can interact with the metal ions. We were somewhat surprised by the pose in which the hydrogen-bearing benzimidazole nitrogen was oriented toward the metal ions but expected that, in reality, tautomerism or rotation of the molecule should allow for a proper orientation of the benzimidazole nitrogen lone pair to interact with the metals. It was therefore decided to test thiabendazole as a possible lead compound in the ecMetAP in vitro assay.

ecMetAP in Vitro Assay. We decided to use the assay procedure described by Yang et al.³ In this method, the oxidation of a fluorogenic substance is coupled to the amount of released methionine and can be measured in a multiplate reader. By switching to an end-point assay, we were able to minimize the influence of possible disturbances such as the presence of other (oxidizing) enzymes, hydrogen peroxide, and a relatively high amount of DMSO during the enzyme reaction. Co^{II} was present at a concentration of 200 μ M. This is in the lower range of metal concentrations used so far. Co^{II} concentrations of 100 μ M³⁰ up to even 1.5 mM³¹ are used in other MetAP assays. Besides thiabendazole, we screened several hundred substances from our in-house compound collection, as well as commercially

Table 1. IC₅₀ Values of 2-Substituted Benzimidazoles on Co^{II}-Loaded ecMetAP

Cpd.: Nr (Name)	R	IC ₅₀ [μM] (% inhibition at 10 μM)
1 (Thiabendazole)		0.472 ± 0.060
2 (Carbendazim)		> 10 (17.597 ± 2.853)
3		> 10 (4.210 ± 2.722)
4		> 10 (5.357 ± 4.983)
5 (Fuberidazole)		> 10 (10.375 ± 3.721)
6		> 10 (30.370 ± 6.262)
7		8.956 ± 1.319
8		0.540 ± 0.028
9		0.574 ± 0.082
10		1.343 ± 0.274
11		0.777 ± 0.033
12		4.591 ± 0.389

available compounds (identified by virtual screening), for their activity against Co^{II}-activated *E. coli* MetAP. We found several substances having activity in the low micromolar range, especially (planar) substances with a known metal binding motif such as 8-hydroxyquinoline or phenanthroline. This was in accordance with our expectations from virtual screening and initially increased our confidence in the docking/scoring results. Thiabendazole was one of the most potent inhibitors with a *K_i* of 400 nM.

Structure–Activity Relationships. Although thiabendazole is not as potent as the lead compound (**42**, Table 5) and its derivatives published earlier by Luo and co-workers,²³ we decided to further investigate some modifications of thiabendazole for several reasons: First, thiabendazole and many other benzimidazole anthelmintics are well-known drugs in clinical practice, and therefore thiabendazole congeners can be expected to have acceptable pharmacokinetic properties. Second, thiabendazole and its derivatives are easily synthesized from substituted diamines and aromatic carboxylic acids and thereby offer quick access to a small library of compounds. Thus, a series of thiabendazole derivatives (compounds **1–41**) has been synthesized and tested to gain insight into the structure–activity relationships for this class of ecMetAP inhibitors. The results are summarized in Tables 1–4.

We first concentrated on the heterocycle in position 2 of the benzimidazole and found that thiazole (**1**) could be substituted by a 1,3-thiazole-2-yl-amine moiety (**8**) or by 2-pyridine (**9**). Other substituents such as 3-pyridine (**3**), 2-thiophene (**4**), 2-furane (**5**), or 2-phenol (**6**) resulted in almost complete loss

Table 2. IC₅₀ Values of N-Alkylated Benzimidazoles on Co^{II}-Loaded ecMetAP

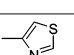
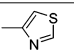
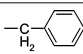
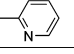
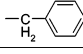
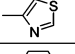
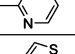
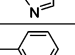
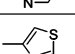
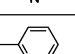
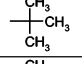
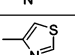
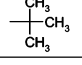
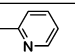
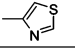
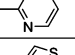
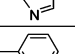
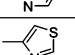
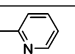
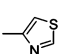
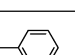
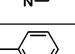
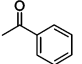
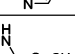
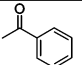
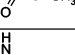
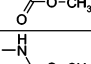
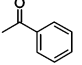
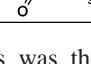
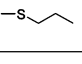
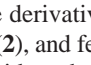
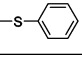
Cpd.	R1	R2	IC ₅₀ [μM] (Inhibition at 10 μM)
13		–CH ₃	0.497 ± 0.007
14			0.461 ± 0.013
15			0.992 ± 0.130

Table 3. IC₅₀ Values of 5- and 6-Substituted Benzimidazoles on Co^{II}-Loaded ecMetAP

Cpd.	R1	R2	R3	IC ₅₀ [μM] (Inhibition at 10 μM)
16		–CH ₃	H	7.157 ± 0.065
17		–CH ₃	H	2.086 ± 0.286
18		–CH ₃	–CH ₃	> 10 (47.767 ± 3.549)
19		–CH ₃	–CH ₃	2.433 ± 0.284
20			H	3.906 ± 0.582
21			H	2.598 ± 0.376
22		–NO ₂	H	1.218 ± 0.128
23		–NO ₂	H	0.162 ± 0.019
24		–NH ₂	H	3.390 ± 0.242
25		–NH ₂	H	0.967 ± 0.024
26		–F	H	4.307 ± 0.635
27		–F	H	1.511 ± 0.192
28		–Cl	H	5.153 ± 1.023
29		–Cl	H	1.695 ± 0.147
30			H	2.397 ± 0.470
31			H	0.403 ± 0.045
32		–CN	H	0.431 ± 0.018
33 (Mebendazole)			H	> 10 (28.987 ± 6.333)
34 (Albendazole)			H	> 10 (15.450 ± 7.193)
35 (Fenbendazole)			H	> 10 (6.067 ± 4.461)

of activity as was the case for the commercially available thiabendazole derivatives mebendazole (**33**), albendazole (**34**), carbendazim (**2**), and fenbendazole (**35**). These compounds have a carbamic acid methyl ester in the 2-position of the benzimi-

Table 4. IC₅₀ Values of Different 2-Substituted Heterocycles Derived from Benzimidazole on Co^{II}-Loaded ecMetAP

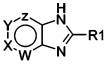
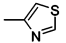
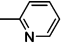
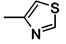
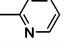
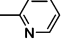
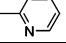
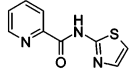
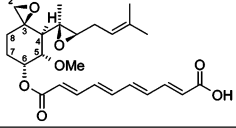
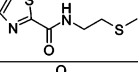
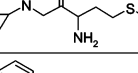
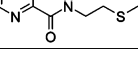
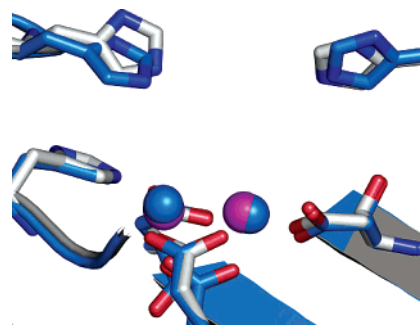
Cpd.	R1					IC ₅₀ [μM] (Inhibition at 10 μM)
		W	X	Y	Z	
36		N	H	H	H	0.078 ± 0.007
37		N	H	H	H	0.105 ± 0.001
38		H	N	H	H	1.724 ± 0.158
39		H	N	H	H	0.550 ± 0.081
40		N	H	N	H	0.376 ± 0.023
41		N	H	H	N	0.240 ± 0.041

Table 5. Known Inhibitors of MetAPs

Cpd.: Nr. (Name)	Formula	IC ₅₀ [μM]
42		0.063 ± 0.011
43 (Fumagilline)		9.152 ± 1.509
44		n.d.
45		n.d.
46		n.d.

dazole system. This indicated that the binding of thiabenzazole and the active congeners is based on interaction with metal ions because it is known that both thiabenzazole and the compound with a (2-)pyridine ring replacing the thiazole ring (**9**) are metal-chelating agents: for both these compounds, metal complexes with different divalent metal ions have been characterized; for thiabenzazole, even Co^{II}-complexes have been synthesized and analyzed.³² Efforts to improve the activity of **9** by adding a hydroxy-group in the 3- or 6-position of the pyridine (**10**, **11**) were unsuccessful and slightly decreased the potency in both cases. Using compound **9** as a secondary lead compound, we next focused on the nitrogen in position 1 of the benzimidazole scaffold. The alkylation of this nitrogen from thiabenzazole had no effect (comps **13** and **14**) but the benzyl derivative (**15**) was slightly less active than the parent compound. These results support the idea that N-3 of the benzimidazole is involved in metal binding and that changing the N-1 substituent has no effect on the binding motif. However, the original aim to reach another binding pocket and to improve the potency by introducing a large substituent at N-1 was not achieved. Next, we investigated the effects of small substituents in the 5- and the 6-position of the benzimidazole moiety (comps **16–32**): Derivatives of the lead compound **9** tolerated substitutions in the 5- and the 6-position better than the corresponding derivatives of thiabenzazole, but most derivatives were less active than the parent compound by a factor from 2 to 5, regardless of which substituent was chosen (halogen, amino, methyl, or dimethyl).

**Figure 3.** Alignment of the Mn^{II}- and the Co^{II}-loaded ecMetAP. The Mn^{II}-loaded form is shown in blue and the Co^{II}-loaded form in magenta/grey. This picture was generated using the program Pymol.³³

Supposing the same binding mode as with thiabenzazole, however, compound **31** shows that even larger substituents can be tolerated and rules out any sterical reasons for the loss of potency observed. The nitrile derivative was slightly more active and also the 5-nitro derivative (**23**) showed an improved potency; it was four times more active than **9**. In contrast, the corresponding 5-nitro-thiabenzazole (**22**) was less active than thiabenzazole. The hint that a polar substituent in position 5 can improve the potency made us try several changes in the benzimidazole scaffold itself, leading to the compounds **36–41**: Introducing a nitrogen in position 5 of the benzimidazole had no effect on the pyridine derivative but decreased the activity of the thiabenzazole derivative. When the position of the nitrogen was shifted from position 5 to 4, the affinity increased independently of the nature of the heterocycle in position 2. Both modified lead compounds (**36** and **37**) had IC₅₀'s in the low nanomolar range (80–100 nM). Other variations of the pyridine derivative yielded no further improvement. Introducing another nitrogen in position 7 and thus changing the benzimidazole into a pyrazine (**41**) decreased the potency to an IC₅₀ value of 240 nM, and changing it into a purine (**40**) resulted in a further decline of the IC₅₀ value to 376 nM.

The potency of MetAP inhibitors has been reported to depend on the identity of the metal ion cofactor.¹⁴ Consequently, we tested a variety of divalent metal ions for their capability to generate a catalytically active ecMetAP. Among Zn^{II}, Mn^{II}, Ni^{II}, Fe^{II}, Fe^{III}, Ca^{II}, and Mg^{II}, only Mn^{II}-MetAP showed activity (about 30% maximum compared to the Co^{II}-MetAP).

Because Mn^{II} was the only metal able to substitute for Co^{II}, all compounds were also tested for their ability to inhibit the Mn^{II}-MetAP. However, none of the compounds was able to inhibit the Mn-enzyme significantly at concentrations up to 10 μM. In addition, neither thiabenzazole nor compounds **9** and **42** showed significant activity in antibacterial assays with *E. coli* as the test organism in concentrations up to 50 μg/mL.

X-ray Crystallography. The structure of the Mn^{II} form of the *E. coli* methionine aminopeptidase complexed with an inhibitor has recently been published by Ye and co-workers (pdb code 1XNZ).¹⁵ When one looks at the substrate and inhibitor differences of the *E. coli* methionine aminopeptidase activated by different metal ions, it seems to be surprising that there is no significant structural difference between the Mn^{II} and the Co^{II} form of the enzyme. The geometry, especially the geometry of the active site conserved residues and the two bound metal ions, is very similar in both the Co^{II} and the Mn^{II} structure (Figure 3) and cannot explain the selectivity of, for example, compounds **1** and **42** for the Co^{II} form of the *E. coli* MetAP.

These findings, together with the failure of thiabenzazole to show in vivo activity, the doubtful reliability of the docking

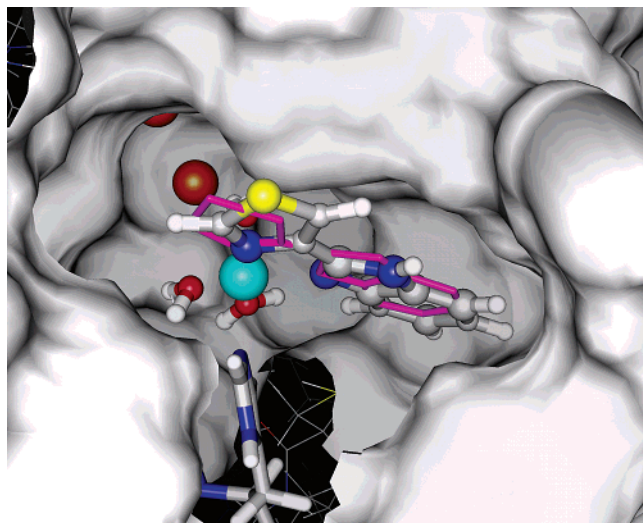


Figure 4. Binding geometries of thiabendazole determined by X-ray crystallography and from docking runs with an auxiliary metal ion. The auxiliary metal is shown in turquoise. The active site has been surfaced except for His79, which binds the auxiliary metal ion. The pose of thiabendazole from docking (GOLD) is shown in ball-and-stick representation with CPK colors, and the X-ray structure is given in stick representation (magenta). In the upper left corner, the two catalytic cobalt ions can (partially) be seen as red spheres.

pose of thiabendazole, and our wish to base further synthetic efforts on a solid structural basis brought us to resolve the crystal structure of thiabendazole bound to Co^{II} -MetAP.

As previously reported,²⁸ we crystallized *E. coli* MetAP in complex with thiabendazole, and the respective three-dimensional structure was determined by X-ray diffraction at a resolution of 1.6 Å (pdb code 1YVM). The binding mode is depicted in Figure 4.

In contrast to our expectations, the two “catalytic” active site metal ions are not involved in the binding of thiabendazole. Rather, an auxiliary third metal ion was present and mediates the binding of thiabendazole to His79. This residue is one of two conserved histidines near the active site and plays an important role in catalysis. The “auxiliary” cobalt ion is complexed in a nearly perfect octahedral geometry by two thiabendazole nitrogens, one histidine nitrogen (His79), and three water molecules.

The same binding mode seems to apply for **42**. This compound was also cocrystallized with the ecMetAP, and the X-ray structure was determined at 1.6 Å. Although the density for the ligand was only partly visible, there was clear density for the additional Co^{II} ion binding at His79. Compound **42** seems to be flipped by 180° compared to thiabendazole, but the position and binding mode of these inhibitors seem to be identical with the adjacent nitrogens complexing the additional Co^{II} ion.

The presence of an additional Co^{II} ion near the active site of *Staphylococcus aureus* MetAP has also been reported by Douangamath.²⁴ In the structures 1QXZ (**44**) and 1QXY (**46**), the auxiliary Co^{II} ion is coordinated by the inhibitors and His178, but the substances also coordinate the two “catalytic” cobalt ions.

In summary, three classes of compounds are known up to now that bind to ecMetAP with a third Co^{II} being present. In two cases, this Co^{II} is essential for the binding of the compounds; in the third, it seems to have (at least) a stabilizing function. Taken together, binding as a metal complex to one of the conserved histidines flanking the active site (His 79 or His 178)

and therefore independent from the active site itself might be the general binding mode for compounds with chelating properties or might at least partly apply for inhibitors of this group.

Structure-Based Interpretation of the SAR Data. The X-ray structure of the thiabendazole–ecMetAP complex enabled us to perform docking runs with the auxiliary cobalt present in the active site. A fundamental problem of molecular docking becomes particularly obvious in this case: the placement of water molecules. The auxiliary cobalt in the thiabendazole complex is ligated by three water molecules, the His79 nitrogen, and two thiabendazole nitrogens. We initially decided to remove all water molecules, but the resulting receptor structure could not be used with the docking software. When a metalloprotein is used as the receptor structure, GOLD identifies possible ligand interaction sites around the metal ions on the basis of the positions of the ligands that are already present in the receptor structure; in our case (without the water molecules), only the histidine nitrogen is present, and it is therefore impossible to unambiguously define octahedral or tetrahedral interaction points for the docked ligands. If, however, the waters are present, then the software is able to spatially define interaction points for metal-binding functional groups, such as carboxylate. The docking result of thiabendazole is shown in Figure 4.

It is obvious that the result closely matches the experimentally determined position of thiabendazole in ecMetAP with an auxiliary cobalt ion. On the basis of this result, the structure–activity relationships can be shortly explained in a structure-based way: Substitution of one of the benzimidazole nitrogens (comps **13–15**) will not affect the activity to a large extent, because these parts of the molecules will protrude from the active site into the solvent (toward the viewer in Figure 4). They are unable to make any additional interactions with the enzyme. Even small extensions of the benzimidazole ring in the 5- or 6-position have a detrimental effect on activity because the fit between the unsubstituted benzimidazole ring and the active site is already very tight. If the substituents in this position exceed a certain size, then a flipping of the molecule must be assumed, which is likely to occur for compound **30** and similar analogues. Any changes to the metal-chelating substructure will abolish activity. Finally, the most active compound in this series (**36**) can make additional hydrogen-bonding interactions to Cys70 (see Figure 5). Although this is not immediately observed from the docking runs with rigid protein, a small reorientation of the cysteine side chain and movement of the inhibitor will bring N4 of the inhibitor into a hydrogen-bonding position relative to the sulfhydryl group of Cys70.

Discrimination of Active and Inactive Compounds by Virtual Screening. Thiabendazole was originally identified by virtual screening. We appreciate this method although it was impossible to foresee the unusual binding mode of thiabendazole and its congeners to ecMetAP. The treatment of metal–ligand interactions within the GOLD software is, in our opinion, one of the best and most useful algorithms available to date. However, the software and its scoring function have been optimized to predict binding poses, and the correlation between GOLD scoring values and measured affinities is generally low. In our case, it is no correlation whatsoever, as can be seen in Figure 6A. The inactive compounds ($\text{IC}_{50} > 10 \mu\text{M}$) cannot be distinguished from the active compounds, and two completely inactive compounds reach the highest score values. Similar results were obtained by using other scoring functions, for example, ChemScore (data not shown). We therefore decided to develop a customizable software for the rescoring of docking

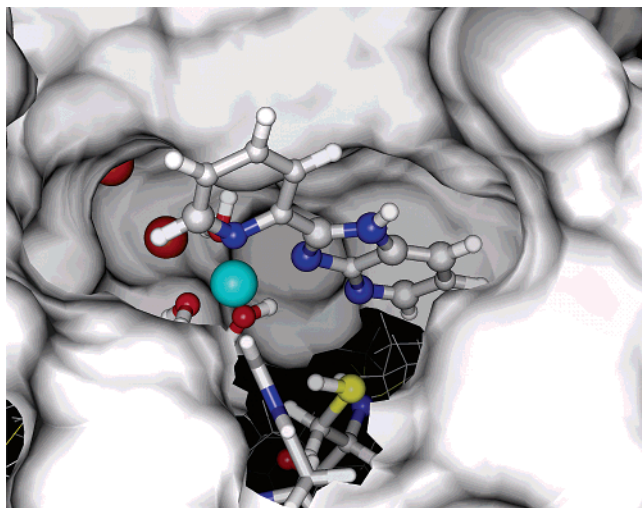


Figure 5. Binding geometry of 37, the most active compound in this series (pose obtained by docking using GOLD). Shown is the solvent-accessible surface of the active site cavity, the auxiliary metal (turquoise), and the His79 and Cys70 residues in ball-and-stick representation.

poses. Since we suspected that the metal–ligand interaction was of particular significance for the binding affinity of these compounds, special emphasis was laid on the customization of heteroatom–metal binding parameters.

TurboScore: Successful Rescoring with Customized Metal-Interaction Parameters. TurboScore is a modular and expandable program system developed by us for rescoring of docking poses generated by docking programs, such as GOLD, FlexX, and AUTODOCK. It reads protein and ligand atom coordinates, as well as atom types and partial charges, from Sybyl mol2-files. It is capable of screening ligands for drug-likeness, for example, by rule-of-five evaluation. The active site of the protein is determined by placing a sphere of a certain radius around the ligand center. All protein atoms inside this sphere belong to the active site. In our study, an active-site radius of 10 Å was used. Afterward a couple of score values such as Coulomb-score, hydrogen bonding-score, and van der Waals-score are generated and finally combined to an overall score.

For prediction of the affinity of the ecMetAP inhibitors presented here we decided to implement a metal interaction term called *metal_contact* into the TurboScore program. The metal interaction term is a contact term evaluating the distance and geometry between potential ligand atoms and metal atoms of the protein active site. A detailed description of the program and the parameters is given in the Experimental Section.

The results obtained by the TurboScore rescoring are shown in Figure 6B. Inactive compounds can be clearly separated from active compounds. In our opinion, this observation highlights the importance of metal interactions for the binding of the compounds described here.

Lack of in Vitro–in Vivo Correlation. Several research groups (refs 23, 24 and 28) have independently reported different inhibitors for all kinds of MetAPs that are highly active in vitro but not in vivo. This lack of in vivo activity has been attributed to pharmacokinetic properties, solubility problems, or the identity of the metal ion used by MetAPs under in vivo conditions. It has been speculated that substitution of Co^{II} by any other metal ion such as Mn^{II} could lead to steric changes in the active site due to different coordination geometries normally observed with the metal ions (octahedral–tetrahedral). The X-ray structure of Mn^{II} -loaded ecMetAP, which is practi-

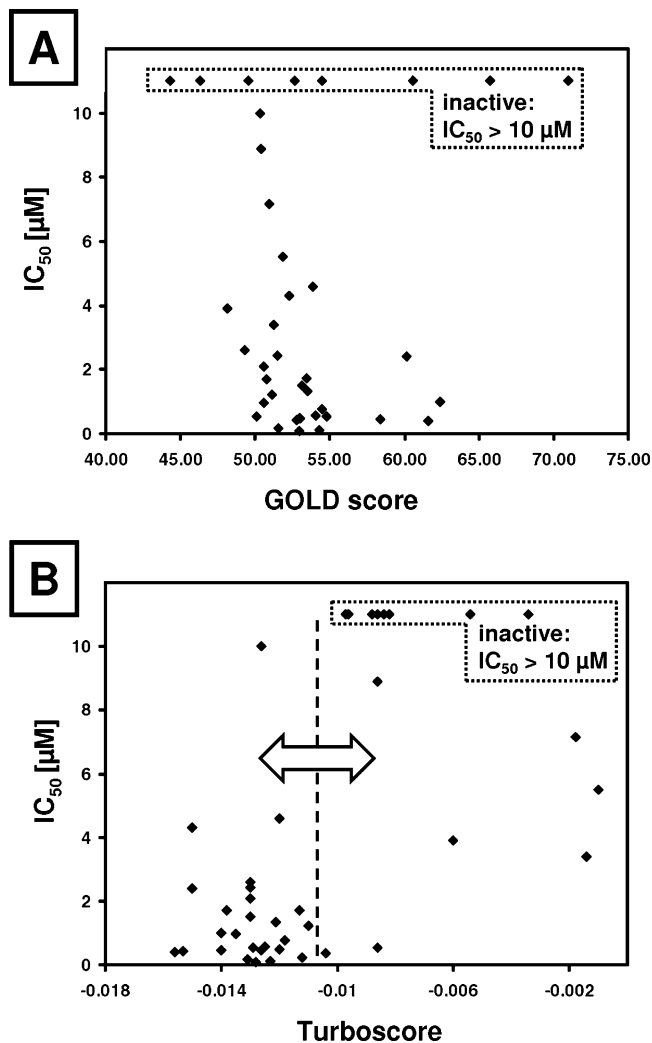


Figure 6. Performance of the GOLD and TurboScore scoring functions in distinguishing active and inactive compounds. Docking was performed on the crystal structure of the thiabendazole/ecMetAP complex without the ligand (pdb 1YVM). All poses were generated using the GOLD software and its “native” scoring function. Rescoring of these poses with the TurboScore scoring function gave the results shown in Figure 6B.

cally superimposable onto the Co^{II} enzyme, makes an end to these speculations. The in vivo inactivity of numerous in vitro active MetAP inhibitors is most probably not related to the identity of the catalytic metal ion, but rather to the unphysiologically high concentration of transition metal ions under in vitro conditions. It is one more example of skewed in vitro results, this time not due to the formation of aggregates by the inhibitors as described in ref 34 but due to the buffer composition.

The binding modes of thiabendazole and compd 42, which both rely on auxiliary cobalt ions, explain the lack of correlation observed between in vitro and in vivo activity. In vitro activity of these compounds must be attributed to the stability of the Co^{II} complex formed and not to steric properties or any kind of interaction of the inhibitor with the enzyme. The selectivity of metal chelating inhibitors for different types of MetAPs might also have been wrongly attributed to the substances themselves but are likely to be a function of their metal complexes.

Another aspect of “chelating” inhibitors concerns their pharmacokinetic properties. Considering the fact that these compounds also form complexes with other divalent metal ions,

they may be "inactivated" within the gastrointestinal tract or the organism by other cations, for example, calcium and magnesium.

Despite these possible explanations, the problem of the in vivo inactivity persists. One could think of using not the chelating inhibitors as such but rather complexed with Co^{II} (or any other of the Co^{II} complexes showing inhibitory effects in vitro) as a drug. These Co^{II} complexes, if sufficiently stable, should be able to inhibit all kind of MetAPs, no matter what the metal in the active site really is, and should thus form a class of compounds with inhibitory potency in different assay systems using different substrates and cofactors. This seems to be a very promising aspect especially regarding the fact that it has not been clearly proven yet what the in vivo metal ion of the MetAPs really is. With the appropriate pharmacokinetic properties, such a complex would also be expected to have in vivo activity.

Future Directions. What are the design principles that should be applied for the future design of in vivo active inhibitors of MetAPs, based upon the work of others and the results presented here? Several structural classes with good in vitro potency can be distinguished, but only a few in vivo active compounds are reported in the literature. Whereas covalent inhibitors inactivate both Co^{II} and Mn^{II} forms of MetAP, the identity of the metal ion has a great influence on the activity of competitive inhibitors. In vivo active competitive inhibitors are frequently based on the bestatin scaffold. They are in vitro active against Mn^{II}-loaded MetAPs type 2 of human but also against Co^{II}-loaded MetAPs.^{12,35,36} Similar inhibitors for the *E. coli* enzyme are known, but the in vivo activity has not been tested.^{14,22} The bestatin-like bengamides are active against Co^{II}-loaded MetAPs and are active in vivo.²⁶ In general, the bestatin-based inhibitors seem to be able to coordinate different metal ions and therefore constitute a promising class of inhibitors. Another class of inhibitors such as 1,2,4-triazoles or pyrazoles seem to be selective for Co^{II} or have only been tested with Co^{II}-loaded MetAPs.^{20,21,37} These substances coordinate to the dimetal center with N1 and N3 of the heterocycle but seem to be inactive against Mn^{II}-MetAP. Although they also seem to be inactive as antibacterial drugs, some analogues inhibit endothelial cell growth, indicating that they are in vivo active inhibitors of MetAP type 2.^{38,39} Only little is known about the metal specificity or in vivo activity for the transition state analogues reported by Doungamath and co-workers.²⁴ Luo et al. published a series of ecMetAP inhibitors that share a pyridine-carboxylic acid moiety with one of the transition state analogues.²³ In addition, these substances possess a heterocycle that forms a metal binding site with a flanking amine group and probably bind in the same way as the benzimidazole analogues reported here. The related di-keto-heterocycles^{15,40} are also Co^{II}-selective substances, and it is likely that they too bind as a complex (and thus are probably inactive in vivo). Recently, furan-carboxylic acid derivatives have been identified that coordinate to the di-Mn^{II} metal center of ecMetAP.¹⁵ It would be interesting to see whether these substances have antibacterial properties.

In summary, there seem to be the following indications for the future design and development of MetAP inhibitors: Structural moieties that can form metal complexes should be avoided, especially chelating elements with two adjacent nitrogens, because these substances seem to be inactive in vivo and normally require auxiliary Co^{II} ions for in vitro activity. Nevertheless, inhibitors should be able to specifically interact with the two "native" active site metal ions. Therefore, a structural motif with a single coordinating moiety (which may,

for example, replace the metal-bridging hydroxide ion) as the central binding group is proposed. As long as the in vivo catalytic metal ion of the different types of MetAPs is not known, the moiety used should not only bind to a specific single kind of metal. To sterically fix the position of this moiety, flanking residues that can interact with the S1 and S1' subsite should be used as has been realized in the bestatins and related inhibitors. Mn^{II} or other suitable metal ions should be used for the screening of inhibitors in parallel to Co^{II}. Thus, substances with inhibitory potency independent from the metal ion could be identified. These compounds are more likely to bind to MetAPs in vivo and produce the desired pharmacological effects.

Conclusions

In summary, thiabendazole was discovered as an ecMetAP inhibitor and various analogues were synthesized and tested. The thiazole cycle could be substituted by 2-pyridine (compound **9**) without loss or improvement of activity, but a complete loss of activity was observed whenever the metal binding moiety was disrupted. Introducing substituent(s) in position 5 or 6 or both had in most cases no beneficial effect. However, changing the benzimidazole scaffold into a benzo[4,5-*b*]pyridine enhanced the potency irrespective of the second, which resulted in two compounds (**21** and **22**) with IC₅₀ values in the lower nanomolar range. The crystal structure of ecMetAP cocrystallized with either thiabendazole or compound **42** revealed a new and surprising binding mode; these substances bind as Co^{II} complexes to His79, a residue that is conserved in all known MetAPs, thus blocking the entrance of the active site. They do not interact with the two catalytic metal ions. This explains the inability of these substances to exert biological activity in vivo because the metal ion concentration in the in vitro assay is considerably higher than that under in vivo conditions. In addition, the activity of these compounds seems to be Co^{II}-specific because Mn^{II} could not take the "auxiliary" place of Co^{II}. By using an adapted scoring function, we were able to distinguish active from inactive compounds in virtual screening procedures. Finally, these results issue a clear warning message to other researchers that are active in the field of metalloprotease inhibitors: a high concentration of metal ions in the assay buffer can lead to artifacts because the inhibitors may be dependent on the artificially high metal concentration.

Experimental Section

Melting points were determined on a Stuart Scientific SMP3, Bibby Sterlin (Essex, United Kingdom) with a heating rate of 6 °C/min. ¹H NMR spectra were recorded on a Bruker DRX-500 spectrometer (500 MHz, Karlsruhe, Germany). Chemical shifts are reported as values (ppm) relative to either internal tetramethylsilane (0 ppm) or the solvent peak. Coupling constants (*J*) are given in Hz. IR spectra were measured with a Vector 33, Bruker (Karlsruhe, Germany), with a Zn/Se ATR unit (ATR Harrick MVP, Software OPUS Version 4.0).

The compounds **1**, **2**, **33**, **34**, **35**, and **43** were purchased from commercial suppliers (Sigma Aldrich) or isolated from commercially available drugs and purified by recrystallization or chromatography on silica gel. The other compounds were prepared by published methods with slight modifications. All chemicals and reagents were of the highest quality available (Sigma, Molecular Probes, Roth, Bachem, Fluka) and were used without further purification.

General Procedures. Procedure A: General Procedures for the Preparation of Substituted Heteroarylbenzimidazoles as Described in Ref 41 for the Compounds 3, 4, 5, 6, 9, 10, 11, 16, 17, 18, 19, 20, 21, 26, 27, 28, 29, 30, 36, 37, 38, and 39. A mixture of an appropriate derivative of *o*-phenyldiamine, the correspond-

ing carboxylic acid, and 5–20 equiv of polyphosphoric acid was stirred in an oil bath at 180 °C for 2 h. The solution was cooled and poured in a thin stream into rapidly stirred water. The pH was adjusted to 9 with 26% ammonium hydroxide. The solid was collected by filtration, dissolved in hot ethanol, and treated with charcoal. The ethanol was evaporated again, and the residue was recrystallized unless stated otherwise.

Procedure B: General Procedure for the Preparation of Substituted Benzimidazoles as Described in Ref 42 for the Compounds 12, 31, 40, and 41. The appropriate diamine, usually as free base, was thoroughly mixed in a mortar with 2 equiv each of anhydrous sodium acetate and the amidine salt. The temperature of the mixture was slowly raised until evolution of ammonia set in, and heating was continued until the melt resolidified. The cake was then treated with 1 N NaOH, and the mixture was decolorized with charcoal and filtered. The hot filtrate was neutralized with glacial acetic acid or by addition of solid ammonium chloride. The product was filtered and recrystallized from water.

Procedure C: General Procedure for the Preparation of N-Alkylated Benzimidazoles as Described in Ref 43 for the Compounds 13, 14, and 15. To a suspension of a suitable benzimidazole (thiabenzazole or compound 9) in dry dimethylformamide and benzene was added a suspension of sodium hydride in benzene. The solution was warmed under nitrogen for 30 min, and then a solution of methyl iodide (or benzyl chloride) in benzene was added dropwise, and the mixture was refluxed under nitrogen for 1 h. The cooled mixture was washed with water, dried over sodium sulfate, and evaporated to dryness to yield crude product.

Procedure D: General Procedure for the Preparation of Nitrated Benzimidazoles as Described in Ref 44 for the compounds 22 and 23. To a solution of a suitable benzimidazole (thiabenzazole or compound 9) in concentrated H₂SO₄ was added concentrated HNO₃ dropwise between 0 and 10 °C. The mixture was stirred at room temperature for 2 h and then poured into ice water. Cautious neutralization with 50% NaOH provided a solid, which was filtered off and crystallized from MeOH to yield the desired product.

Procedure E: Reduction on Pd/Charcoal as Described in Ref 45 for the Compounds 24 and 25. One gram of a nitro derivative was dissolved in 100 mL of absolute ethanol, and the solution was reduced catalytically over 0.5 g of 10% palladium-on-charcoal at normal pressure and room temperature. After the uptake of hydrogen was complete, the catalyst was removed by filtration, and the solvent was evaporated in vacuo. Upon recrystallization, the pure compounds were obtained.

Procedure F: General Procedure for the Preparation of Esters and Amides as Described in Ref 46. A suitable amine or alcohol (25 mmol), pyridine (44 mmol), and a suitable sulfonyl or carboxyl chloride (26 mmol) were heated on a steam bath for 2 h and then poured into water. The resulting precipitate was collected and recrystallized.

Specific Compounds. Compound 7: Method as Described in Ref 47. *O*-Phenylenediamine (1.94 g, 0.018 mol) and 5-amino-3*H*-1,2,4-dithiazole-3-thione (3.3 g, 0.022 mol, known as isoperthiocyanic acid) in absolute ethanol (30 mL) were refluxed for 22 h. The solvent was distilled from the reaction mixture, and the residue was treated with aqueous sodium hydroxide (1 N, 3 × 25 mL) and then filtered. The filtrate was carefully neutralized to pH 7 and kept in a refrigerator for 8 h. The white precipitate (3.22 g, 96%) that had formed was collected, washed with water, and dried.

Compound 8: Method as Described in Ref 48. To a stirred and refluxing suspension of (1*H*-benzimidazol-2-yl)-thiourea (3.64 mmol) in water (3 mL) was added dropwise 1,2-dichloroethyl ethyl ether (3.86 mmol). After 2 h, the cooled mixture was basified (NaOH). The product was filtered and recrystallized from aqueous EtOH.

Compound 32: Method as Described in Refs 49 and 50. A stirred solution of pyridine-2-carbaldehyde (85.7 mg, 0.8 mmol) and 3,4-diamino-benzonitrile (100 mg, 0.75 mmol) in 8 mL of nitrobenzene was heated at 145 °C under N₂ overnight. The cooled reaction mixture was treated with 3% HCl (3 × 25 mL), and the

pH was adjusted to 8 with NH₄OH. The voluminous precipitate was filtered and then purified by column chromatography (EtOAc/hexane 1:1) to give 32.

Compound 42: Prepared as Described in Ref 23. In short, to a mixture of pyridine-2-carboxylic acid (10 mmol), thiazol-2-ylamine (10 mmol), and HOBT (10.75 mmol) in dry DMF (10 mL) was added DCC (10.05 mmol). The reaction mixture was diluted with 50 mL of EtOAc and 20 mL of H₂O. The aqueous phase was extracted with EtOAc. The combined organic phases were washed with 10% aqueous HCl, water, and brine, dried over anhydrous MgSO₄ and chromatographed (3:1 petroleum ether/EtOAc) to yield 42 (73%).

Preparation of Starting Materials. Thiazole-4-carboxylic Acid. At first, bromopyruvic acid was prepared according to ref 51. One mole of pyruvic acid was heated to 50 °C in a three-neck flask equipped with ground glass joints, and 1 mol of bromine, previously dried by shaking with concentrated H₂SO₄, was added dropwise with stirring and exclusion of moisture. The heat of the reaction was usually sufficient to keep the temperature at 50 °C; external temperature control was resorted to when necessary. The thick fuming syrup was immediately poured into a large crystallizing dish, the flask was washed with a small amount of hot benzene, and the washing was added to the main product. Sometimes the material set in the flask to a fuming crystal mass, which was dissolved in a small amount of hot benzene. The mixture was placed in a vacuum desiccator over moist NaOH pellets, and the solvent was removed by suction. On the next day, the material was ground to a fine powder and kept in vacuo over NaOH pellets for 48–72 h with frequent renewal of the alkali until no more fumes of HBr were given off. The yield was 85% of white crystals melting at 70 °C.

The thiazole-4-carboxylic acid was then prepared using a modification of procedures in ref 52 as described in ref 53. To a stirred solution of 7.75 g (172 mmol) of formamide in 250 mL of THF, which was cooled to 0 °C, was added all at once 13.2 g (30 mmol) of solid P₄S₁₀. After this addition, the ice bath was removed, and the reaction was stirred at 30 °C for 3 h. The resultant mixture was cooled to room temperature, filtered, and added to a solution of 2.7 g (16.2 mmol) of 3-bromopyruvic acid in some THF. The mixture was then heated to 40–50 °C for 3 h, and a precipitate started to appear. After cooling, the precipitate was filtered off and dissolved in some water with concentrated H₂SO₄, the pH was adjusted to pH 2–3 with NaOH, and the product precipitated as a white solid in the refrigerator. Yields were normally about 22%. ¹H NMR (500 MHz, *d*₆-DMSO): δ (ppm) 8.53 (1H, s), 9.17 (1H, s).

Pyridine-2-carboxamide hydrochloride and pyrazine-2-carboxamide hydrochloride were prepared as described in ref 54. A solution of 26.0 g (0.25 mol) of 2-cyanopyridine (or 2-cyanopyrazine) and 1.35 g (0.025 mol) of sodium methoxide in 25 mL of methanol was allowed to stand overnight at room temperature. The amidine salt has then been prepared in situ from the imidate with an amount of ammonium chloride equivalent to the total base present. The reaction mixture was merely stirred for a few hours until the salt dissolved. The reaction time varied from 1 to 24 h. The solvent methanol was evaporated to recover the amidine salt that was used without further purification.

Pyrazine-2,3-diamine was prepared as described in refs 55–57. A solution of pyrazinecarboxamide (24.6 g, 0.20 mol) in 90% formic acid (100 mL) and 30% hydrogen peroxide (62.5 mL) was stirred and heated. The temperature was kept between 40 and 50 °C for 4 h and then at 40 °C for 1 h. A colorless solid started to separate from the solution after heating for approximately 10 min. The mixture was refrigerated overnight, then filtered, washed with water, and dried to give 59% (lit. 66%) of the *N*-oxide, mp 306–306 °C. This material was used directly in successive transformations without further purification.

Sodium hypochlorite solution (4.0 mmol/mL available chlorine) was added dropwise to a stirred solution of sodium hydroxide (8.08 g, 0.20 mmol) in water (125 mL) at room temperature. The amide (6.956 g, 0.050 mmol) was added in one portion to the above

solution, and the resulting mixture was heated at 70 °C with stirring for 1 h. During this period, the amide dissolved. After cooling below 20 °C, the solution was acidified to pH 0 with concentrated hydrochloric acid and then again basified at pH 9–10 with 2 N NaOH. The mixture was evaporated to dryness in vacuo, and the residue was powdered and extracted with chloroform by a Soxhlet extractor for 24 h to give 70% (lit. 78%) of 3-aminopyrazine-1-oxide, mp 177–178 °C.

To 1 mmol of the oxide, which was stirred under nitrogen, MeCN (8 cm³), trimethylsilyl azide (0.17 cm³, 1.2 mmol), and finally diethylcarbamoyl chloride (0.16 cm³, 1.2 mmol) were added via syringe. The mixture was stirred under reflux for 18 h and then evaporated under reduced pressure. The residue was subjected to chromatography on silica gel eluting with hexanes–EtOAc (10:1 to 3:1) and gave 2-amino-3-azidopyrazine in 92% yield (lit. 99%), mp 225 °C.

A mixture of the azidopyrazine (1 mmol) and tin(II) chloride dehydrate (1.128 g, 5 mmol) in 12 N HCl (3.0 mL) and MeOH (3.0 mL) was stirred and heated at 60 °C until the starting material was completely consumed. After cooling to rt, the solution was basified with solid Na₂CO₃ to pH 8–9 and then evaporated to dryness in vacuo. The residue was extracted with EtOAc while hot or by Soxhlet apparatus, and the extract was dried (MgSO₄). Evaporation and chromatography on silica gel gave 2,3-diaminopyrazine, 70% (lit. 87%), mp 207–209 °C. The diamine was used without further purification.

The TurboScore Program. First, parameters such as the maximum and the minimum possible contact distances (contact_tol_max, contact_tol_min) are read in from standard input. These parameters were set to 3.2 and 1.7 Å respectively. Afterward the parameter file for atom type dependent scoring was read in and the total number of metal atoms was detected. The parametrization used in this study is shown in Table 6.

For each possible ligand atom the contact distance d_{ML} toward the metal atom is calculated by eq 1, where ΔML_x , ΔML_y and ΔML_z are the metal–ligand atom distances in the x , y , and z direction.

$$d_{ML} = \left(\begin{matrix} \Delta ML_x \\ \Delta ML_y \\ \Delta ML_z \end{matrix} \right) = \sqrt{\Delta ML_x^2 + \Delta ML_y^2 + \Delta ML_z^2} \quad (1)$$

A metal–ligand contact is formed if d_{ML} is within the range contact_tol_min and contact_tol_max. For this contact, a score value is calculated. There are three types of distance-dependent score potentials available in TurboScore, two experimental type potentials (eqs 2 and 3) and one modified Lennard-Jones type potential (eq 4). The choice of the score potential is dependent on the target protein and the type of metal atom.

$$\text{score_model1}(d_{ML}) = 30(d_{ML} - \text{contact_tol_min})^2 e^{-4(d_{ML} - \text{contact_tol_min})} \quad (2)$$

$$\text{score_model2}(d_{ML}) = 3(d_{ML} - \text{contact_tol_min})^2 e^{-1.1(d_{ML} - \text{contact_tol_min})^2} \quad (3)$$

$$\text{score_model3}(d_{ML}) = \frac{90}{d_{ML}^{12}} - \frac{10}{d_{ML}^8} \quad (4)$$

In this study, the modified Lennard-Jones type potential was used. The original Lennard-Jones type potential is a 12–6 potential, and it is widely used to describe nonbonding interactions such as van der Waals interactions. Here, we use a 12–8 potential because of the better performance describing the metal interactions. The score of the contact is obtained by multiplication with the atom type parameter given in Table 6 (eq 5).

$$\text{score} = \text{score_model} \times \text{atom_type_parameter} \quad (5)$$

Finally, score-values of all possible metal–ligand contacts are summarized leading to the conclusive metal-contact score.

Table 6. Atom-Type-Dependent Parametrization of the Metal Interaction Term of TurboScore

Sybyl atom type	Value
O.CO2	1
O.2	0.2
O.3	0.15
N.3	0.8
N.2	0.6
N.1	0.6
N.ar	0.6
N.am	0.6
N.p3	0.6
S.3	0.6
S.2	0.6

Enzyme Preparation: Expression and Purification of *E. coli* MetAP. A C-terminal poly-His-tagged form of *E. coli* MetAP was obtained by overexpression in *E. coli* using an Arg-175-Gln mutant kindly provided by Prof. W. T. Lowther and Prof. B. Matthews.⁵⁸

Four liter fermentation cultures of BL21(DE3) *E. coli* cells containing the expression plasmid were grown in Luria–Bertani broth with kanamycin (100 mg/L) at 37 °C and 250 rpm. Expression was induced after cooling to 25 °C by the addition of isopropyl β -D-thiogalactoside to 1 mM at 0.8–1.0 OD₆₀₀. The cells were allowed to grow for another 3 h at 25 °C. The cells were centrifuged at 8500 rpm and 4 °C for 15 min, resuspended in medium, and centrifuged again at 4500 rpm and 4 °C for 15 min. The pellet was frozen at –80 °C and crushed in a mortar while being cooled with liquid nitrogen. The resulting powder was suspended in 100 mL of an altered +T/G buffer at 4 °C [50 mM Hepes, pH 7.9/10% glycerol/0.1% Triton X-100/0.5 M KCl/5 mM imidazole and additionally 40 μ g/mL DNase/1 mM MgCl₂/15 mM methionine/1 mM PMSF], and the cells were lysed in a French press at 1.0 kbar. The resulting solution is then centrifuged at 40 000 \times g at 4 °C for 30 min. The supernatant was loaded onto a 10-mL nitrilotriacetic acid–agarose column (Qiagen) equilibrated with +T/G buffer. After washing with +T/G buffer and –T/G buffer (–T/G buffer without glycerol, Triton X-100, and inhibitor cocktail), MetAP was eluted at 4 °C with about 160 mL of –T/G buffer containing 60 mM imidazole directly into 1 mL of 500 mM EDTA, pH 8.0. Additional EDTA was added, if necessary, to give a final concentration of 5 mM. After overnight dialysis at 4 °C against 25 mM Hepes buffer, pH 7.9, 150 mM KCl, and 15 mM methionine, MetAP was concentrated to a volume of about 30 mL (corresponding to a protein concentration of 20 mg/mL) and stored at –80 °C. The poly-His-tail was removed by incubation of 100 mg of MetAP with 0.1–1 U/mg of thrombin (Novagen)/2.5 mM CaCl₂ at 15 °C for 18–20 h. Passage of the protein through another nitrilotriacetic acid–agarose column equilibrated with –T/G buffer resulted in His-tag free protein; the volume was reduced to 3 mL, and the MetAP was subsequently loaded onto a Superdex 75 Hi-load, pregrade 16/60 gel filtration column (Pharmacia) equilibrated with 25 mM Hepes, pH 7.1, 25 mM K₂SO₄, and 100 mM NaCl and further purified. Protein concentrations were determined by absorption at 280 nm with the extinction coefficient of 16 350 M^{–1}cm^{–1} (1.89 mg/mL). Typical yields were 100–150 mg/L of culture.

Determination of IC₅₀ Values. Assays were performed in 96-well microtiter plates (Greiner) using the method of Yang et al.³ In a typical assay, MetAP (28 μ L, 75 nM, 50 mM tris/maleate, pH 7.5, 0.1% BSA) was preincubated with CoCl₂ (20 μ L, 2 mM, tris/maleate, pH 7.5), buffer (54.8 μ L, 50 mM tris/maleate, pH 7.5), NaCl (20 μ L, 1 M), and BSA (17.2 μ L, 1% in 50 mM tris/maleate, pH 7.5) and with inhibitor (20 μ L, different concentrations in 50 mM tris/maleate buffer, pH 7.5, containing 1% DMSO) or without inhibitor (20 μ L, 50 mM tris/maleate buffer, pH 7.5 containing 1% DMSO) for 30 min at 37 °C. Then, the reaction was started by the

addition of MGMM (40 μL , 1 mM) resulting in a total volume of 200 μL with the following concentrations: MetAP 10.5 nM, CoCl₂ 200 μM , NaCl 100 mM, BSA 0.1%, and MGMM 200 μM . The reaction was stopped after 15 min at 37 °C by adding a mixture of EDTA/Amplex Red reagent (29.5 μL of 76.3 mM EDTA and 0.5 μL of Amplex 5 mM). Detection was started with the addition of a mixture of horseradish peroxidase/L-amino acid oxidase (16 μL of 0.065 625 U/ μL HRP and 4 μL of 0.001 875 U/ μL AAO) resulting in a total volume of 250 μL and the following concentrations: 9 mM EDTA, 10 μM Amplex, 1.05 U HRP, and 0.0075 U AAO. The resulting fluorescence was measured using a Wallac Victor2 multiplate reader (Greiner, filters λ_{ex} =544 nm, λ_{em} =590 nm) for 90 min and corrected by the corresponding zero values. The IC₅₀ values were obtained by calculating the mean value of three independent measurements. Reagents and buffers were prepared in deionized MilliQ-filtered water.

Analytical Data. 2-Pyridin-3-yl-1H-benzimidazol (3): Method A. Light purple solid, yield 93%, mp 245 °C, recrystallized twice from ethanol. C₁₂H₉N₃ (195.23). Anal. (C₁₂H₉N₃) C calcd, 73.83; found, 71.22; H calcd, 4.65; found, 5.62; N calcd, 21.52; found, 23.17.

2-Thiophen-2-yl-1H-benzimidazol (4): Method A. Light brown solid, yield 80%, mp 344 °C, recrystallized from ethanol. C₁₁H₈N₂S (200.26). Anal. (C₁₁H₈N₂S) C, H calcd, 4.03; found, 4.54; N calcd, 13.99; found, 13.47.

2-Furan-2-yl-1H-benzimidazol (5): Method A. Light yellow needles, yield 40%, mp 286 °C, purified by column chromatography (EtOAc–hexane 1 + 1.5) and recrystallized from ethanol. C₁₁H₈N₂O (184.20). Anal. (C₁₁H₈N₂O) C, H, N.

2-(1H-Benzimidazol-2-yl)-phenol (6): Method A. Light gray-green solid, yield 40%, mp 242 °C, recrystallized from ethanol. C₁₃H₁₀N₂O (210.24). Anal. (C₁₃H₁₀N₂O) C, H, N.

1H-Benzimidazol-2-yl-thiourea (7). White solid, yield 92%, mp 196–198 °C, purification not necessary. C₈H₈N₄S (192.24). Anal. (C₈H₈N₄S) C calcd, 49.98; found, 50.50; H, N calcd, 29.14; found, 28.39.

(1H-Benzimidazol-2-yl)-thiazol-2-yl-amin (8). White solid, yield 85%, mp 252–254 °C, recrystallized from aqueous EtOH. C₁₀H₈N₄S (216.27). Anal. (C₁₀H₈N₄S) C calcd, 55.54; found 56.09; H, N calcd, 25.91; found, 25.27.

2-Pyridin-2-yl-1H-benzimidazol (9): Method A. White solid, yield 93%, mp 224 °C, recrystallized from ethanol and washed with hexane. C₁₂H₉N₃ (195.23). Anal. (C₁₂H₉N₃) C, H, N.

6-(1H-Benzimidazol-2-yl)-pyridin-2-ol (10): Method A. White solid, yield 46%, mp 284–285 °C, washed with some hot ethanol. C₁₂H₉N₃O (211.23). Anal. (C₁₂H₉N₃O) C, H, N.

2-(1H-Benzimidazol-2-yl)-pyridin-3-ol (11): Method A. Light-grey solid, yield 98%, mp 189 °C, purification not necessary. C₁₂H₉N₃O (211.23). Anal. (C₁₂H₉N₃O) C calcd, 68.24; found 67.39; H calcd, 4.29; found 4.72; N calcd, 19.89; found, 20.31.

2-Pyrazin-2-yl-1H-benzimidazol (12): Method B. Yellow solid, yield 85%, mp 242–244 °C, recrystallized from aqueous EtOH. C₁₁H₈N₄ (196.21). Anal. (C₁₁H₈N₄) C, H, N.

1-Methyl-2-thiazol-4-yl-1H-benzimidazol (13): Method C. White solid, yield 79%, mp 150 °C, purified over silica gel (EtOAc) and recrystallized from EtOH. C₁₁H₉N₃S (215.28). Anal. (C₁₁H₉N₃S) C, H, N calcd, 19.52; found, 18.93.

1-Benzyl-2-thiazol-4-yl-1H-benzimidazole (14): Method C. White solid, yield 35%, mp 146 °C, purified over silica gel (EtOAc–hexane 1 + 2). C₁₇H₁₃N₃S (291.38). Anal. (C₁₇H₁₃N₃S) C, H calcd, 4.50; found, 5.14; N calcd, 14.42; found, 13.46.

1-Benzyl-2-pyridin-2-yl-1H-benzimidazole (15): Method C. White solid, yield 47%, mp 116–118 °C, purified over silica gel with EtOAc–hexane 1 + 3. C₁₉H₁₅N₃ (285.35). Anal. (C₁₉H₁₅N₃) C, H, N.

5-Methyl-2-thiazol-4-yl-1(3H)-benzimidazole (16): Method A. Brown solid, yield 52%, mp 240–241 °C, recrystallized from aqueous EtOH. C₁₁H₉N₃S (215.28). Anal. (C₁₁H₉N₃S) C, H, N.

5-Methyl-2-pyridin-2-yl-1(3H)-benzimidazol (17): Method A. Brown solid, yield 77%, mp 164 °C, purification not necessary.

C₁₃H₁₁N₃ (209.25). Anal. (C₁₃H₁₁N₃) C calcd, 74.62; found, 74.13; H calcd, 5.30; found, 5.74; N.

5,6-Dimethyl-2-thiazol-4-yl-1H-benzimidazole (18): Method A. Brown solid, yield 74%, mp 247–249 °C, recrystallized from aqueous EtOH. C₁₂H₁₁N₃S (229.31). Anal. (C₁₂H₁₁N₃S) C, H, N.

5,6-Dimethyl-2-pyridin-2-yl-1H-benzimidazole (19): Method A. Light-brown solid, yield 86%, mp 193 °C, purification not necessary. C₁₄H₁₃N₃ (223.28). Anal. (C₁₄H₁₃N₃) C, H, N.

5-tert-Butyl-2-thiazol-4-yl-1H-benzimidazol (20): Method A. Grey-brown solid, yield 50%, mp 165–168 °C, recrystallized from aqueous EtOH. C₁₄H₁₅N₃S (257.36). Anal. (C₁₄H₁₅N₃S) C, H, N.

5-tert-Butyl-2-pyridin-2-yl-1H-Benzimidazole (21): Method A. Grey solid, yield 59%, mp 151 °C, recrystallized from aqueous EtOH. C₁₆H₁₇N₃ (252.33). Anal. (C₁₆H₁₇N₃) C, H, N.

5-Nitro-2-thiazol-4-yl-1(3H)-benzimidazole (22): Method D. Light yellow solid, yield 55%, mp 242 °C, recrystallized from EtOH. C₁₀H₆N₄O₂S (246.25). Anal. (C₁₀H₆N₄O₂S) C, H, N.

5-Nitro-2-pyridin-2-yl-1(3H)-benzimidazol (23): Method D. Light yellow solid, yield 43%, mp 213–214 °C, recrystallized from MeOH. C₁₂H₈N₄O₂ (240.22). Anal. (C₁₂H₈N₄O₂) C, H, N.

5-Amino-2-thiazol-4-yl-1H-benzimidazol (24): Method E. Light yellow solid, yield 62%, mp 233–235 °C, recrystallized from aqueous ethanol. C₁₀H₈N₄S (216.27). Anal. (C₁₀H₈N₄S) C, H, N calcd, 25.91; found, 25.27.

2-Pyridin-2-yl-3H-benzimidazol-5-ylamine (25): Method E. Light yellow solid, yield 80%, mp 217 °C, recrystallized from EtOH. C₁₂H₁₀N₄ (210.24). Anal. (C₁₂H₁₀N₄) C calcd, 68.56; found, 69.05; H, N calcd, 26.65; found, 26.05.

5-Fluor-2-thiazol-4-yl-1H-benzimidazol (26): Method A. Brown-red solid, yield 76%, mp 260–261 °C, recrystallized from aqueous EtOH. C₁₀H₆FN₃S (219.24). Anal. (C₁₀H₆FN₃S) C, H, N.

6-Fluoro-2-pyridin-2-yl-1H-benzimidazole (27): Method A. Dark purple solid, yield 96%, mp 181 °C, purification not necessary. C₁₂H₈FN₃ (213.22). Anal. (C₁₂H₈FN₃) C calcd, 67.60; found, 67.11; H, N calcd, 19.71; found, 20.21.

5-Chlor-2-thiazol-4-yl-1H-benzimidazol (28): Method A. Grey solid, yield 56%, mp 238–240 °C, recrystallized from aqueous EtOH. C₁₀H₆ClN₃S (235.70). Anal. (C₁₀H₆ClN₃S) C, H, N.

5-Chloro-2-pyridin-2-yl-1(3H)-benzimidazole (29): Method A. White solid, yield 49%, mp 141 °C, extracted with hot benzene and treated with charcoal, then purified over silica gel (EtOAc) and recrystallized from benzene. C₁₂H₈ClN₃ (229.67). Anal. (C₁₂H₈ClN₃) C, H calcd, 3.51; found, 4.07; N.

Phenyl-(2-thiazol-4-yl-1H-benzimidazol-5-yl)-methanone (30): Method A. Light yellow solid, yield 35%, mp 95–98 °C, purified over silica gel (EtOAc–hexane 1 + 2.5) and recrystallized from aqueous ethanol. C₁₇H₁₁N₃OS (305.36). Anal. (C₁₇H₁₁N₃O) C, H, N.

Phenyl-(2-pyridin-2-yl-3H-benzimidazol-5-yl)-methanone (31): Method B. Light yellow solid, yield 20%, mp 73–76 °C, not soluble in 1 N NaOH; therefore the cake was dissolved in EtOH, and the product was precipitated with water and then recrystallized from aqueous EtOH. C₁₉H₁₃N₃O (299.33). Anal. (C₁₉H₁₃N₃O) C calcd, 76.24; found, 75.72; H, N.

2-Pyridin-2-yl-3H-benzimidazole-5-carbonitrile (32). White solid, yield 36%, mp 216–218 °C, purified over silica gel (EtOAc–hexane 1 + 1). C₁₃H₈N₄ (220.24). Anal. (C₁₃H₈N₄) C calcd, 70.90; found, 72.54; H, N calcd, 25.44; found, 23.46.

2-Thiazol-4-yl-1H-imidazo[4,5-b]pyridine (36): Method A. Purple solid, yield 97%, mp 306 °C, purification not necessary. C₉H₆N₄S (202.24). Anal. (C₉H₆N₄S) C, H, N.

2-Pyridin-2-yl-1H-imidazo[4,5-b]pyridine (37): Method A. Brown solid, yield 46%, mp 242–243 °C, recrystallized from EtOH. C₁₁H₈N₄ (196.21). Anal. (C₁₁H₈N₄) C calcd, 67.34; found, 66.79; H, N calcd, 28.55; found, 29.05.

2-Thiazol-4-yl-1H-imidazo[4,5-c]pyridine (38): Method A. White solid, yield 98%, mp 273 °C, purification not necessary. C₉H₆N₄S (202.24). Anal. (C₉H₆N₄S) C, H, N.

2-Pyridin-2-yl-1H-imidazo[4,5-c]pyridine (39): Method A. White solid, yield 78%, mp 232 °C, recrystallized from EtOH. C₁₁H₈N₄ (196.21). Anal. (C₁₁H₈N₄) C calcd, 67.34; found, 67.82; H, N.

8-Pyridin-2-yl-7(9)H-purine (40): Method B. White solid, yield 62%, mp 289–291 °C, recrystallized from H₂O. C₁₀H₇N₅ (197.20). Anal. (C₁₀H₇N₅) C calcd, 60.91; found, 61.63; H, N calcd, 35.51; found, 34.72.

2-Pyridin-2-yl-1H-imidazo[4,5-b]pyrazine (41): Method B. Light brown solid, yield 69%, mp 306–309 °C, recrystallized from aqueous ethanol, C₁₀H₇N₅ (197.20). Anal. (C₁₀H₇N₅) C calcd, 60.91; found, 61.96; H calcd, 3.58; found, 2.96; N calcd, 35.51; found, 35.08.

Acknowledgment. We thank Professor R. Hartmann for his continued support of our work. This project was supported by the Deutsche Forschungsgemeinschaft (Grant KL 1356) and the Fonds der Chemischen Industrie.

Supporting Information Available: Analytical characterization of compounds 3–32 and 36–41 and a table containing elemental analyses of compounds 1–42. This material is available free of charge via the Internet at <http://pubs.acs.org>.

References

- World Health Organization, The World Health Report 2004: Changing History. http://www.who.int/whr/2004/en/report04_en.pdf, 2004.
- Ben-Bassat, A.; Bauer, K.; Chang, S. Y.; Myambo, K.; Boosman, A.; Chang, S. Processing of the initiation methionine from proteins: properties of the *Escherichia coli* methionine aminopeptidase and its gene structure. *J. Bacteriol.* **1987**, *169* (2), 751–757.
- Yang, G.; Kirkpatrick, R. B.; Ho, T.; Zhang, G. F.; Liang, P. H.; Johanson, K. O.; Casper, D. J.; Doyle, M. L.; Marino, J. P., Jr.; Thompson, S. K.; Chen, W.; Tew, D. G.; Meek, T. D. Steady-state kinetic characterization of substrates and metal-ion specificities of the full-length and N-terminally truncated recombinant human methionine aminopeptidases (type 2). *Biochemistry* **2001**, *40* (35), 10645–10654.
- Dummitt, B.; Fei, Y.; Chang, Y. H. Functional expression of human methionine aminopeptidase type 1 in *Saccharomyces cerevisiae*. *Protein Pept. Lett.* **2002**, *9* (4), 295–303.
- Liu, S.; Widom, J.; Kemp, C. W.; Crews, C. M.; Clardy, J. Structure of human methionine aminopeptidase-2 complexed with fumagillin. *Science* **1998**, *282* (5392), 1324–1327.
- Chang, S. Y.; McGary, E. C.; Chang, S. Methionine aminopeptidase gene of *Escherichia coli* is essential for cell growth. *J. Bacteriol.* **1989**, *171* (7), 4071–4072.
- Li, X.; Chang, Y. H. Amino-terminal protein processing in *Saccharomyces cerevisiae* is an essential function that requires two distinct methionine aminopeptidases. *Proc. Natl. Acad. Sci. U.S.A.* **1995**, *92* (26), 12357–12361.
- Miller, C. G.; Kukral, A. M.; Miller, J. L.; Movva, N. R. pepM is an essential gene in *Salmonella typhimurium*. *J. Bacteriol.* **1989**, *171* (9), 5215–5217.
- Bradshaw, R. A.; Brickey, W. W.; Walker, K. W. N-terminal processing: the methionine aminopeptidase and N alpha-acetyl transferase families. *Trends Biochem. Sci.* **1998**, *23* (7), 263–267.
- Klein, C. D.; Schiffmann, R.; Folkers, G.; Piana, S.; Rothlisberger, U. Protonation states of methionine aminopeptidase and their relevance for inhibitor binding and catalytic activity. *J. Biol. Chem.* **2003**, *278* (48), 47862–47867.
- Walker, K. W.; Bradshaw, R. A. Yeast methionine aminopeptidase I can utilize either Zn²⁺ or Co²⁺ as a cofactor: a case of mistaken identity? *Protein Sci.* **1998**, *7* (12), 2684–2687.
- Wang, J.; Sheppard, G. S.; Lou, P.; Kawai, M.; Park, C.; Egan, D. A.; Schneider, A.; Bouska, J.; Lesniewski, R.; Henkin, J. Physiologically relevant metal cofactor for methionine aminopeptidase-2 is manganese. *Biochemistry* **2003**, *42* (17), 5035–5042.
- D'Souza V. M.; Holz, R. C. The methionyl aminopeptidase from *Escherichia coli* can function as an iron(II) enzyme. *Biochemistry* **1999**, *38* (34), 11079–11085.
- Li, J. Y.; Chen, L. L.; Cui, Y. M.; Luo, Q. L.; Li, J.; Nan, F. J.; Ye, Q. Z. Specificity for inhibitors of metal-substituted methionine aminopeptidase. *Biochem. Biophys. Res. Commun.* **2003**, *307* (1), 172–179.
- Ye, Q. Z.; Xie, S. X.; Huang, M.; Huang, W. J.; Lu, J. P.; Ma, Z. Q. Metalloform-selective inhibitors of *Escherichia coli* methionine aminopeptidase and X-ray structure of a Mn(II)-form enzyme complexed with an inhibitor. *J. Am. Chem. Soc.* **2004**, *126* (43), 13940–13941.
- Hanson, F. R.; Eble, T. E. An antipheage agent isolated from aspergillus. *J. Bacteriol.* **1949**, *58*, 527–529.
- McCowen, M. C.; Callender, M. E.; Lawlis, J. F. Fumagillin (H-3), a New Antibiotic with Amebicidal Properties. *Science* **1951**, *113*, 202–203.
- Killough, J. H.; Magill, G. B.; Smith, R. C. The treatment of amebiasis with fumagillin. *Science* **1952**, *115* (2977), 71–72.
- Ingber, D.; Fujita, T.; Kishimoto, S.; Sudo, K.; Kanamaru, T.; Brem, H.; Folkman, J. Synthetic analogues of fumagillin that inhibit angiogenesis and suppress tumour growth. *Nature* **1990**, *348*, 555–557.
- Oefner, C.; Douangamath, A.; D'Arcy, A.; Hafeli, S.; Mareque, D.; MacSweeney, A.; Padilla, J.; Pierau, S.; Schulz, H.; Thormann, M.; Wadman, S.; Dale, G. E., The 1.15 Å crystal structure of the *Staphylococcus aureus* methionyl-aminopeptidase and complexes with triazole based inhibitors. *J. Mol. Biol.* **2003**, *332* (1), 13–21.
- Garrabrant, T.; Tuman, R. W.; Ludovici, D.; Tominovich, R.; Simoneaux, R. L.; Galemno, R. A., Jr.; Johnson, D. L. Small molecule inhibitors of methionine aminopeptidase type 2 (MetAP-2). *Angiogenesis* **2004**, *7* (2), 91–96.
- Hu, X.; Zhu, J.; Srivathsan, S.; Pei, D. Peptidyl hydroxamic acids as methionine aminopeptidase inhibitors. *Bioorg. Med. Chem. Lett.* **2004**, *14* (1), 77–79.
- Luo, Q. L.; Li, J. Y.; Liu, Z. Y.; Chen, L. L.; Li, J.; Qian, Z.; Shen, Q.; Li, Y.; Lushington, G. H.; Ye, Q. Z.; Nan, F. J. Discovery and structural modification of inhibitors of methionine aminopeptidases from *Escherichia coli* and *Saccharomyces cerevisiae*. *J. Med. Chem.* **2003**, *46* (13), 2631–2640.
- Douangamath, A.; Dale, G. E.; D'Arcy, A.; Almstetter, M.; Eckl, R.; Frutos-Hoener, A.; Henkel, B.; Ilgen, K.; Nerdinger, S.; Schulz, H.; MacSweeney, A.; Thormann, M.; Trembl, A.; Pierau, S.; Wadman, S.; Oefner, C. Crystal structures of *Staphylococcus aureus* methionine aminopeptidase complexed with keto heterocycle and aminoketone inhibitors reveal the formation of a tetrahedral intermediate. *J. Med. Chem.* **2004**, *47* (6), 1325–1328.
- Keding, S. J.; Dales, N.; Lim, S.; Beaulieu, D.; Rich, D. H. Synthesis of (3R)-Amino-(2S)-hydroxy Amino Acids for Inhibition of Methionine Aminopeptidase-I. *Synth. Commun.* **1998**, *28*, 4463–4470.
- Towbin, H.; Bair, K. W.; DeCaprio, J. A.; Eck, M. J.; Kim, S.; Kinder, F. R.; Morollo, A.; Mueller, D. R.; Schindler, P.; Song, H. K.; van Oostrum, J.; Versace, R. W.; Voshol, H.; Wood, J.; Zabludoff, S.; Phillips, P. E. Proteomics-based target identification: bengamides as a new class of methionine aminopeptidase inhibitors. *J. Biol. Chem.* **2003**, *278* (52), 52964–52971.
- Klein, C. D.; Folkers, G. Understanding the selectivity of fumagillin for the methionine aminopeptidase type II. *Oncol. Res.* **2003**, *13* (12), 513–520.
- Schiffmann, R.; Heine, A.; Klebe, G.; Klein, C. D. Metal Ions as Cofactors for the Binding of Inhibitors to Methionine Aminopeptidase: A Critical View of the Relevance of In Vitro Metalloenzyme Assays. *Angew. Chem., Int. Ed.* **2005**, *44* (23), 3620–3623.
- Huang, C. C.; Couch, G. S.; Pettersen, E. F.; Ferrin, T. E. Chimera: An Extensible Molecular Modeling Application Constructed Using Standard Components. <http://www.cgl.ucsf.edu/chimera>. *Pac. Symp. Biocomput.* **1996**, *1*, 724.
- Zhou, Y.; Guo, X. C.; Yi, T.; Yoshimoto, T.; Pei, D. Two continuous spectrophotometric assays for methionine aminopeptidase. *Anal. Biochem.* **2000**, *280* (1), 159–165.
- Griffith, E. C.; Su, Z.; Niwayama, S.; Ramsay, C. A.; Chang, Y. H.; Liu, J. O. Molecular recognition of angiogenesis inhibitors fumagillin and ovalicin by methionine aminopeptidase 2. *Proc. Natl. Acad. Sci. U.S.A.* **1998**, *95* (26), 15183–15188.
- Mothilal, K. K.; Karunakaran, C.; Rajendran, A.; Murugesan, R. Synthesis, X-ray crystal structure, antimicrobial activity and photodynamic effects of some thiabendazole complexes. *J. Inorg. Biochem.* **2004**, *98* (2), 322–332.
- DeLano, W. L. The PyMOL Molecular Graphics System on World Wide Web, <http://www.pymol.org>, 2002.
- McGovern, S. L.; Caselli, E.; Grigorieff, N.; Shoichet, B. K. A common mechanism underlying promiscuous inhibitors from virtual and high-throughput screening. *J. Med. Chem.* **2002**, *45* (8), 1712–1722.
- Wang, J.; Sheppard, G. S.; Lou, P.; Kawai, M.; BaMaung, N.; Erickson, S. A.; Tucker-Garcia, L.; Park, C.; Bouska, J.; Wang, Y. C.; Frost, D.; Tapang, P.; Albert, D. H.; Morgan, S. J.; Morowitz, M.; Shusterman, S.; Maris, J. M.; Lesniewski, R.; Henkin, J. Tumor suppression by a rationally designed reversible inhibitor of methionine aminopeptidase-2. *Cancer Res.* **2003**, *63* (22), 7861–7869.
- Sheppard, G. S.; Wang, J.; Kawai, M.; BaMaung, N. Y.; Craig, R. A.; Erickson, S. A.; Lynch, L.; Patel, J.; Yang, F.; Searle, X. B.; Lou, P.; Park, C.; Kim, K. H.; Henkin, J.; Lesniewski, R. 3-Amino-2-hydroxyamides and related compounds as inhibitors of methionine aminopeptidase-2. *Bioorg. Med. Chem. Lett.* **2004**, *14* (4), 865–868.

- (37) Chen, L. L.; Li, J.; Li, J. Y.; Luo, Q. L.; Mao, W. F.; Shen, Q.; Nan, F. J.; Ye, Q. Z. Type I methionine aminopeptidase from *Saccharomyces cerevisiae* is a potential target for antifungal drug screening. *Acta Pharmacol. Sin.* **2004**, *25* (7), 907–914.
- (38) Corporation, S. B.; Kallander, L. S.; Ryan, M. D.; Thompson, S. K. Compounds and methods. World patent WO 03/051906 A2, 06.06.2003, 2003.
- (39) Marino, J. P. J.; Thompson, S. K.; Veber, D. F. Compounds and methods. International Patent Application PCT/US04/0116490 A1, 17.06.2004, 2004.
- (40) Li, J. Y.; Chen, L. L.; Cui, Y. M.; Luo, Q. L.; Gu, M.; Nan, F. J.; Ye, Q. Z. Characterization of full length and truncated type I human methionine aminopeptidases expressed from *Escherichia coli*. *Biochemistry* **2004**, *43* (24), 7892–7898.
- (41) Lee, I.-S. H.; Jeoung, E. H.; Lee, K. L. Synthesis and tautomerism of 2-aryl and 2-heteroaryl derivatives of benzimidazole. *J. Heterocycl. Chem.* **1996**, *33*, 1711–1716.
- (42) Bergmann, F. G.; Kleiner, M. A.; Rashi, M. New Substituted Purines and Purine Derivatives. U.S. Patent 1,201,997A, 1968.
- (43) Maynard, J. A.; Rae, I. D.; Rash, D.; Swan, J. M. Reaction of 2-(4'-Thiazolyl)Benzimidazole (Thiabendazole) with alkyl halides. *Aust. J. Chem.* **1971**, *24*, 1873–1881.
- (44) Haugwitz, R. D.; Maurer, B. V.; Jacobs, G. A.; Narayanan, V. L.; Cruthers, L.; Szanto, J. Antiparasitic agents. 3. Synthesis and anthelmintic activities of novel 2-pyridinyl-5-isothiocyanatobenzimidazoles. *J. Med. Chem.* **1979**, *22* (9), 1113–1118.
- (45) Sarett, L. H.; Brown, H. D. 5-(or 6)-Halo(or Amino)benzazoles and methods for preparing same. U.S. Patent 3,478,046, 1969.
- (46) Clark-Lewis, J. W.; Thompson, M. J. Methylation of 3-Aminopyridines and Preparation of 2-Amino-3-methylaminopyridine and 2:3-Diaminopyridine. *J. Chem. Soc.* **1957**, 442–446.
- (47) Krishnaswamy, N. R.; Sundaresan, C. N. 5-Amino-3H-1,2,4-dithiazole-3-thione as a synthon: New synthesis of 2-thioureidobenzothiazoles. *Heteroat. Chem.* **1994**, *5* (5/6), 567–569.
- (48) Jen, T.; Van Hoesen, H.; Groves, W.; McLean, R.; Loev, B. Amidines and related compounds. 6. Studies on structure–activity relationships of antihypertensive and antisecretory agents related to clonidine. *J. Med. Chem.* **1975**, *18* (1), 90–99.
- (49) Kim, J. S.; Yu, C.; Liu, A.; Liu, L. F.; LaVoie, E. J. Terbenzimidazoles: influence of 2ⁿ-, 4-, and 5-substituents on cytotoxicity and relative potency as topoisomerase I poisons. *J. Med. Chem.* **1997**, *40* (18), 2818–2824.
- (50) Sun, Q.; Gatto, B.; Yu, C.; Liu, A.; Liu, L. F.; LaVoie, E. J. Synthesis and evaluation of terbenzimidazoles as topoisomerase I inhibitors. *J. Med. Chem.* **1995**, *38* (18), 3638–3644.
- (51) Sprinson, D. B.; Chargaff, E. A Study of β -Hydroxy- α -Keto Acids. *J. Biol. Chem.* **1946**, *164*, 417–432.
- (52) Jagoe, C. T. Ph.D. Thesis, Boston College, 1991, pp 154–288.
- (53) Kumar, S.; Pearson, A. L.; Pratt, R. F. Design, synthesis, and evaluation of alpha-ketoheterocycles as class C beta-lactamase inhibitors. *Bioorg. Med. Chem.* **2001**, *9* (8), 2035–2044.
- (54) Schaefer, F. C.; Peters, G. A. Base-Catalyzed Reaction of Nitriles with Alcohols. A Convenient Route to Imidates and Amidine Salts. *J. Org. Chem.* **1961**, *26*, 412–417.
- (55) Sato, N. Studies on pyrazines. 18. A new and convenient synthesis of 2-amino-3-cyanopyrazine. *J. Heterocycl. Chem.* **1989**, *26*, 817–819.
- (56) Sato, N.; Miwa, N.; Hirokawa, N. Studies on pyrazines. Part 27. A new deoxidative nucleophilic substitution of pyrazine *N*-oxides; synthesis of azidopyrazines with trimethylsilyl azide. *J. Chem. Soc., Perkin Trans. 1* **1994**, 885–888.
- (57) Sato, N.; Matsuura, T.; Miwa, N. Studies on pyrazines. Part 30: Synthesis of aminopyrazines from azidopyrazines. *Synthesis* **1994**, *9*, 931–934.
- (58) Lowther, W. T.; McMillen, D. A.; Orville, A. M.; Matthews, B. W. The anti-angiogenic agent fumagillin covalently modifies a conserved active-site histidine in the *Escherichia coli* methionine aminopeptidase. *Proc. Natl. Acad. Sci. U.S.A.* **1998**, *95* (21), 12153–12157.

JM050476Z